Adaptive *hp*-Refinement for 2-D Maxwell Eigenvalue Problems: Method and Benchmarks

Jake J. Harmon, *Graduate Student Member, IEEE*, and Branislav M. Notaroš, *Fellow, IEEE*

***Abstract*—We present an application of goal-oriented adaptive isotropic *hp*-refinement for the 2-D Maxwell eigenvalue problem. We apply a simplified goal-oriented error expression for improving the accuracy of the eigenvalues, which, when combined with indicators derived from the solution, enables highly targeted discretization tuning. Furthermore, we introduce an *hp*-refinement/coarsening optimizer coupled with error smoothness estimation for refinement classification and execution. These enhancements yield cost-effective resource allocations that reach extremely high accuracy rapidly even for eigenvalues of singular eigenfunctions. Finally, we provide numerical benchmarks more accurate than existing numerical reference values, along with new benchmarks for higher-order modes that will facilitate the comparison and development of new approaches to adaptivity and *hp* finite elements in computational electromagnetics (CEM). Our implementation is based on the open-source finite element library deal.II.**

***Index Terms*—adjoint methods, adaptive error control, adaptive refinement, computational electromagnetics, finite element method, higher order methods, hp-refinement.**

I. Introduction

In the presence of singular—or generally non-smooth behavior—p-refinement, the process of increasing the polynomial order of the discretization, yields only algebraic convergence; yet with a sufficiently smooth solution, p-refinement provides exponential convergence. Combined hp-refinement, however, which controls the resolution of the domain subdivision and the expansion orders, enables exponential convergence even for non-smooth solutions, unlocking significant potential for accuracy and efficiency for general problems in computational electromagnetics (CEM) and electromagnetic modeling.

The development and application of hp capable methods is of increasing interest in CEM and the broader applied mathematics community. As the demands for accuracy increase, the need for enhanced convergence, and therefore the substitution of low-order methods with higher-order alternatives, has driven significant development for practical applications in hp-refinement.

Constructing the most accurate and efficient discretization demands versatility in the model, such as non-uniform cell sizes and non-uniform expansion orders. Such versatility, however, requires adequate adaption and refinement instruction for practical and effective applications. To ensure a rapidly convergent adaptive mesh refinement (AMR) procedure, we target the discretization with goal-oriented error estimation. As opposed to standard strategies, which either specifically examine the accuracy of the solution or some property of the solution as a surrogate for the accuracy, the dual weighted residual (DWR) expression of the error enables rigorous error estimation related to quantities of interest (QoIs) computed from the solution. Furthermore, we augment the utility of the dual weighted residual by extracting the field error for smoothness estimation, which facilitates significantly improved convergence and consistency in comparison to smoothness estimation of the solution itself.

Goal-oriented error estimation and adaptive refinement remains a key focus of research in the applied mathematics community. For a comprehensive overview, with a particular emphasis on duality-based approaches, see [1]–[3].

Mixed-order and hp-methods were introduced in [4]–[7], demonstrating that under proper conditions, exponential convergence with respect to the number of degrees of freedom may be achieved through a combination of h- and p-refinements. Since then, many practical studies of hp capable methods have followed, e.g., [8], [9]. Furthermore, open-source libraries such as deal.II [10], [11] have alleviated many of the practical hurdles of implementing hp-methods, yet challenges remain for effective application.

Considering the Maxwell eigenvalue problem, which is the focus of this manuscript, the success of adaptive error control approaches naturally relies on the convergence of the discrete problem to the continuous problem; rigorous analyses of this convergence through proofs of the discrete compactness property have shown the viability of $H(\text{curl})$-conforming Galerkin discretizations for solving the Maxwell eigenvalue problem with h-refinement procedures in [12], p-refinement procedures in [13], and combined hp-refinement procedures in [14]. Previously, [15] studied the application of p-refinement for a variety of waveguide models. For adaptive hp-refinement, an analysis of a standard residual-based error indicator and convergence was conducted in [16]. Similarly, [17], [18] studied exponential rates of convergence for cavity resonators and manual discretization refinements for smooth and singular eigenfunctions.

The predominate approach for hp-refinement of Maxwell equation problems in CEM, however, has relied mostly on multi-grid techniques, with iterative construction and comparison of a starting discretization and a globally refined (simultaneously in h and in p) reference, such as in [19]–[21]. Additionally, in [22] hp-refinement was applied according to this approach for accurate S-parameter computation of waveguide discontinuities with energy-norm minimization refinement and, as an extension of the energy-norm approach, goal-

Manuscript received May 10, 2021, revised November 22, 2021; accepted December 28, 2021.

Jake J. Harmon and Branislav M. Notaroš are with the department of Electrical and Computer Engineering, Colorado State University, Fort Collins, CO 80523-1373 USA (e-mail: jake.harmon@ieee.org, branislav.notaros@colostate.edu).

oriented strategies. A similar study of goal-oriented adaptivity for S-parameter computation was conducted in [23]. Notably, [24] proved convergence in the energy norm for a residual-based hp-refinement algorithm while also avoiding the high computational cost of the above multi-grid techniques, with applications to a variety of Maxwell equation problems in the 3-D finite element method (FEM).

Other approaches in applied mathematics have leveraged, in addition to various types of error estimation or indication, estimation of several characteristics of the discretization to determine the choice between h- and p-refinement. In [7], local error indicators were computed for a base mesh and its globally p-refined realization, with the ratio of these error indicators deciding whether to h- or p-refine. On the other hand, in [25] the smoothness of the solution was estimated from the Legendre expansion. Similarly, [26] studied the decay rate of the Fourier and Legendre series expansions to guide hp-refinement. Additionally, in [27], the Sobolev regularity of the solution was estimated from the Legendre expansion coefficients. We pursue the approach of estimating the decay rate of Legendre coefficients to generate a smoothness indicator; however, we study the smoothness of the error field (i.e., the estimated difference between the exact solution and its approximation), rather than the solution itself, to better target the discretization error and insufficient local smoothness.

Similar error estimates through the DWR were also applied to 1-D dielectric slab problems [28], and to accelerated p-refinement for electromagnetic scattering problems in 3-D FEM [29]. Instead, we provide a simplified form for the DWR of the Maxwell eigenvalue problem for eigenvalue QoIs and combined hp-refinement. Moreover, in this paper we explore attaining maximal accuracy through hp-refinement optimization, which, in addition to ease of use, results in exponential convergence with respect to the number of degrees of freedom.

The rest of this paper is organized as follows. Section II outlines the construction of the simplified error estimate and the hp-refinement classification procedures. Section III provides numerical examples, illustrating the strong performance of the proposed refinement procedure for the Maxwell eigenvalue problem in 2-D FEM. The examples indicate attainment of exponential rates of convergence even for eigenvalues of singular eigenfunctions. Lastly, we provide improved numerical benchmarks for a challenging waveguide model.

II. Error Estimation and Refinement Classification

A. Problem Formulation

We first outline the Maxwell eigenvalue problem. From the source-free Maxwell equations (in differential form), we have the following problem involving the electric field $\mathbf{E}$,

$$\nabla \times (\mu_r^{-1} \nabla \times \mathbf{E}) - k_0^2 \varepsilon_r \mathbf{E} = 0 \text{ in } \Omega, \tag{1}$$

where μ_r and ε_r denote the relative permeability and permittivity of the medium, respectively, and k_0 denotes the free space wavenumber.

We now impose several practical constraints on the types of problems we will study. First, let us assume Ω describes a very long, uniform perfect electrical conductor (PEC) waveguide filled with air (i.e., $\mu_r = 1$ and $\varepsilon_r = 1$), resulting in the Dirichlet boundary condition

$$\hat{\mathbf{n}} \times \mathbf{E} = 0 \text{ on } \partial\Omega, \tag{2}$$

where $\hat{\mathbf{n}}$ denotes the direction normal to the boundary.

The electric field in the waveguide varies spatially according to

$$\mathbf{E} = \mathbf{E}(x, y) e^{-\gamma z}, \tag{3}$$

where γ denotes the propagation constant, which is, in general, complex valued. Lastly, for the purposes of establishing benchmarks, we investigate only the transverse electric (TE) modes (i.e., the electric field in the axial direction is zero). The procedure can be repeated identically for transverse magnetic (TM) modes by isolating the magnetic field intensity $\mathbf{H}$ instead. As the objective of the numerical method (and therefore the adaptivity) is the accurate and efficient computation of the cutoff-frequencies, we let $\gamma = 0$.

Naturally, physical eigenpairs of (1) correspond to those with eigenvalues greater than zero. Moreover, the eigenfunctions of positive eigenvalues automatically satisfy the divergence condition $\nabla \cdot \mathbf{E} = 0$. Spurious modes, which cluster exclusively around zero, may be eliminated trivially in post-processing, or the outlined approach may be augmented to a mixed finite element method to enforce the divergence condition [30].

The aforementioned problem—when reduced to a 2-D cross-section—admits the following variational form after Galerkin testing: Find $U_{hp} = \{\mathbf{u}_{hp}, \lambda_{hp}\} \in B_{hp} \times \mathbb{R}_{>0}$ such that

$$a(\mathbf{u}_{hp}, \boldsymbol{\phi}_{hp}) = \lambda_{hp} m(\mathbf{u}_{hp}, \boldsymbol{\phi}_{hp}) \quad \forall \boldsymbol{\phi}_{hp} \in B_{hp}, \tag{4}$$

with $a(\mathbf{u}_{hp}, \boldsymbol{\phi}_{hp}) = \langle \nabla_t \times \mathbf{u}_{hp}, \nabla_t \times \boldsymbol{\phi}_{hp} \rangle$ (where ∇_t represents the transversal gradient operator and $\langle \cdot, \cdot \rangle$ denotes the standard L^2 inner-product), and $m(\mathbf{u}_{hp}, \boldsymbol{\phi}_{hp}) = \langle \mathbf{u}_{hp}, \boldsymbol{\phi}_{hp} \rangle$, for a finite dimensional subspace $B_{hp} \subset H_0(\text{curl}; \Omega)$, where $H_0(\text{curl}; \Omega) = \{ \mathbf{u} \in H(\text{curl}; \Omega) \mid \hat{\mathbf{n}} \times \mathbf{u} = 0 \text{ on } \partial\Omega \}$ and $\Omega \subset \mathbb{R}^2$.

With the preceding problem constraints, we restrict our analysis to the 2-D Maxwell eigenvalue problem; nevertheless, the same approach could be applied to the 3-D Maxwell eigenvalue problem directly (assuming access to the prerequisite 3-D hp-refinement infrastructure). We note, however, that the general waveguide problem requires a more complicated variational formulation than (4), as described in, e.g., [15], [31].

Finally, letting $U = \{\mathbf{u}, \lambda\} \in H_0(\text{curl}; \Omega) \times \mathbb{R}_{>0}$ denote the exact solution to the generalized eigenvalue problem, we are interested in the approximation error of the eigenvalue λ_{hp}, i.e., the difference

$$e_{\lambda_{hp}} \coloneqq \lambda - \lambda_{hp}. \tag{5}$$

In the remainder of this paper, we study the adaptive control of this error through automated refinements of the underlying discretization of the forward problem.

B. Error Estimation

To apply the DWR procedure for the generalized eigenvalue problem in order to compute (5) in such a way as to guide adaptive error control, we first require an appropriate functional of the solution that, in this case specifically, permits relating the properties of the discretization and the accuracy of an eigenvalue. However, as any scalar multiple of an eigenvector is also an eigenvector, we first assert a convenient normalization condition for the eigenfunction. Specifically, as in [32], we choose $\mathbf{u}$ such that

$$\langle \mathbf{u}, \mathbf{u} \rangle = 1, \tag{6}$$

and likewise for the approximate solution $\mathbf{u}_{hp}$, which amounts to normalizing the eigenfunctions according to the L^2-norm.

We then take the functional

$$J[U] = \lambda \langle \mathbf{u}, \mathbf{u} \rangle = \lambda, \tag{7}$$

which, in concert with the normalization condition (6), produces the desired QoI and, as a result, we have that

$$J[U] - J[U_{hp}] = e_{\lambda_{hp}}. \tag{8}$$

To derive explicit expressions for the QoI error and refinement indicators, we follow the procedure in [32]. Given the above formulation and constraints, the associated dual eigenvalue problem for considering an eigenvalue QoI is identical to the forward problem, i.e., (4) is self-adjoint. Based on [32], we can construct a simplified form of the QoI error, namely

$$e_{\lambda_{hp}}(1-\sigma_{hp}) = a(\mathbf{u}_{hp}, \mathbf{u}-\boldsymbol{\psi}_{hp}) - \lambda_{hp} m(\mathbf{u}_{hp}, \mathbf{u}-\boldsymbol{\psi}_{hp}), \tag{9}$$

for arbitrary $\boldsymbol{\psi}_{hp} \in B_{hp}$, with $\sigma_{hp} = \frac{1}{2} m(\mathbf{u}-\mathbf{u}_{hp}, \mathbf{u}-\mathbf{u}_{hp})$. While any choice of $\boldsymbol{\psi}_{hp}$ preserves the identity (9) (due to Galerkin orthogonality), we choose $\boldsymbol{\psi}_{hp} = \boldsymbol{\Pi}^{\text{curl}}_{hp}\mathbf{u}$, the curl-conforming projection-based interpolation (see [33] and the references therein for a detailed description of this operator) of $\mathbf{u}$ into the original primal finite element space, to excise the unimportant information in accumulating the error estimate, which, as opposed to other choices (e.g., $\boldsymbol{\psi}_{hp} = 0$), enhances the utility of the error indicators for refinement.

The contributions in (9) are accumulated separately for each cell K such that the total error is equivalent to

$$\begin{aligned} e_{\lambda_{hp}}(1-\sigma_{hp}) = &\sum_K a_K(\mathbf{u}_{hp}, \mathbf{u}-\boldsymbol{\psi}_{hp}) \\ &- \lambda_{hp} m_K(\mathbf{u}_{hp}, \mathbf{u}-\boldsymbol{\psi}_{hp}), \end{aligned} \tag{10}$$

where the subscript K indicates that the integral terms a and m are evaluated just over the cell K.

To enhance the control of discretization error (particularly related to that of the approximation at the boundaries of the cells), the contributions are then separated into a cell residual and boundary residual. Integration by parts reveals that

$$\begin{aligned} a_K(\mathbf{u}, \mathbf{v}) = &\int_{\Omega_K} (\nabla \times \nabla \times \mathbf{u}) \cdot \mathbf{v} \, d\Omega_K \\ &- \int_{\partial\Omega_K} (\nabla \times \mathbf{u}) \times \mathbf{v} \cdot \hat{\mathbf{n}} \, dS_K, \end{aligned} \tag{11}$$

with $\hat{\mathbf{n}}$ denoting the direction normal to the boundary as in (2). Note that the second integral in (11) is performed over the boundary of the cell (i.e., along the edges in 2-D and over the faces in 3-D).

In the case of the boundary term for a given cell, we average its contribution with the boundary terms from the neighboring cells to instead measure the jump of the tangentially directed curl $\nabla \times \mathbf{u}_{hp}$ (which is, in general, discontinuous) weighted by $\mathbf{u} - \boldsymbol{\psi}_{hp}$, i.e.,

$$\begin{aligned} e_{\lambda_{hp}}(1-\sigma_{hp}) = &\sum_K \langle \nabla \times \nabla \times \mathbf{u}_{hp}, \, \mathbf{u}-\boldsymbol{\psi}_{hp} \rangle_K \\ &- \frac{1}{2} \big[\langle \hat{\mathbf{n}} \times (\nabla \times \mathbf{u}_{hp}), \, \mathbf{u}-\boldsymbol{\psi}_{hp} \rangle_{\partial K} \\ &\quad - \langle \hat{\mathbf{n}} \times (\nabla \times \mathbf{u}_{hp}), \, \mathbf{u}-\boldsymbol{\psi}_{hp} \rangle_{\partial K'} \big] \\ &- \lambda_{hp} m_K(\mathbf{u}_{hp}, \mathbf{u}-\boldsymbol{\psi}_{hp}) \\ = &\sum_K \tilde{\eta}_K, \end{aligned} \tag{12}$$

where K' indicates the collection of cells that share an edge (in 2-D) or a face (in 3-D) with cell K, and $\tilde{\eta}_K$ denotes the final error contribution estimate associated with cell K. In implementation, this procedure amounts to traversing each cell to compute the volume terms and a separate traversal of every face/edge, accumulating the contributions from the cells on either side as described in (12). Furthermore, note that for the combination of two boundary terms as in (12), the curl of the forward solution must be evaluated on both sides of an edge (or a face in 3-D); however, given its tangential continuity, $\mathbf{u} - \boldsymbol{\psi}_{hp}$ may be evaluated just once for each edge/face.

Finally, in addition to error indicators for refinement, the summation of the signed contributions $\tilde{\eta}_K$ from each cell K provides a correction term—by means of (9)—to improve the accuracy of the approximate eigenvalue computed from the forward problem. For the purposes of refinement in the remainder of the paper, we define the refinement *indicator* η_K to be the absolute value of the error contribution estimate $\tilde{\eta}_K$, i.e.,

$$\eta_K \coloneqq |\tilde{\eta}_K|, \tag{13}$$

for each cell K.

In the above expressions, we assume access to the exact solution $\mathbf{u}$. In general, however, we must substitute an approximation of $\mathbf{u}$. Galerkin orthogonality precludes taking $\mathbf{u}_{hp}$ as the approximation for $\mathbf{u}$, as it would imply an estimate of zero error. Instead, we replace $\mathbf{u}$ with a finite dimensional approximation $\mathbf{u}_{hp^+} \in B_{hp^+}$, where B_{hp^+} denotes the enriched finite element space generated by increasing the expansion orders of each cell by one in the discretization of the forward problem (4). While very effective for error estimation, alternative approaches, such as those discussed in [1], can provide improvements in efficiency.

C. Refinement Classification

Following the above error estimation procedure yields a collection of cells cataloged according to their estimated contributions to the QoI error. To approach optimally equilibrated discretizations during the convergence procedure, we develop

a variant of the selection scheme introduced in [34]. Since the primary concern is that the local regularity of the solution prevents accelerated convergence, for the purposes of designing the marking scheme, let us temporarily assume we h-refine only. Furthermore, in this manuscript we consider only isotropic refinements in h and p, while additional efficiency and versatility may be unlocked through anisotropic refinements (though with greater requirements of the underlying refinement and coarsening infrastructure) [35].

We consider the marking procedure as a two-step process, with an independent refinement step, followed by a coarsening step. We have, therefore, in concert with the trinary marking decision, three groups of cells to treat: the m cells to refine, the l cells to coarsen, and the remaining cells which are left unchanged. Under one h-refinement step, the number of new cells introduced when refining the m cells with the largest error contribution estimates is

$$\left(2^d - 1\right) m, \tag{14}$$

where d denotes the geometric dimension of the discretization. Grouping cells into the set of refined cells, R, and unrefined cells, $\tilde{R}$, the total predicted error η after an h-refinement step is

$$\eta = \sum_{K \in R} 2^{-\alpha(K)} \eta_K + \sum_{K \in \tilde{R}} \eta_K, \tag{15}$$

where $\alpha(K)$ denotes the predicted rate of convergence on cell K, which we take as the degree of the polynomial basis on the cell (i.e., ignoring the regularity in the convergence condition), with an associated refinement indicator η_K produced from (12) by means of (13). From [34], the refinement procedure must weight not just the error reduction, but also the increased cost and, as a result, should minimize the following objective function

$$\begin{aligned} J_{refine}(m) = N_{\alpha_1}^{\alpha_1/d} \left(\sum_{\substack{K \in R(m) \\ \alpha(K) = \alpha_1}} 2^{-\alpha_1} \eta_K + \sum_{\substack{K \in \tilde{R}(m) \\ \alpha(K) = \alpha_1}} \eta_K \right) + \cdots \\ + N_{\alpha_j}^{\alpha_j/d} \left(\sum_{\substack{K \in R(m) \\ \alpha(K) = \alpha_j}} 2^{-\alpha_j} \eta_K + \sum_{\substack{K \in \tilde{R}(m) \\ \alpha(K) = \alpha_j}} \eta_K \right), \end{aligned} \tag{16}$$

where, to track the increased cost of refining higher-order cells, N_{α_i} counts the number of cells (after refinement) that have a polynomial basis of degree α_i, for $i = 1, \ldots, j$, where j denotes the number of different expansion orders in the discretization. The optimal m cells with the largest error contributions may be found through simple enumeration. Hence, for marking cells for refinement, the approach ensures the best choice—according to the objective function (16)—for the worst-case scenario (h-refinement only).

In the interest of practicality, we enforce the coarsening as a succession to refinement (rather than a parallel operation). Analogous to the case of refinement, the coarsening procedure should seek to minimize the predicted error increase while maximizing the computational savings. In tandem with this goal, any coarsening procedure should accelerate error homogenization to improve discretization quality and efficiency. With the set R (the refined cells) fixed, we consider reclassifying the unrefined cells for coarsening by determining the l cells with the smallest error contribution estimates that minimize

$$\begin{aligned} J_{coarsen}(l) = N_{\alpha_1}^{\alpha_1/d} \left(\sum_{\substack{K \in \tilde{R}(l) \\ \alpha(K) = \alpha_1}} \eta_K + \sum_{\substack{K \in \hat{R}(l) \\ \alpha(K) = \alpha_1}} 2^{\alpha_1} \eta_K \right) + \cdots \\ + N_{\alpha_j}^{\alpha_j/d} \left(\sum_{\substack{K \in \tilde{R}(l) \\ \alpha(K) = \alpha_j}} \eta_K + \sum_{\substack{K \in \hat{R}(l) \\ \alpha(K) = \alpha_j}} 2^{\alpha_j} \eta_K \right), \end{aligned} \tag{17}$$

where $\hat{R}$ indicates the set of cells marked for coarsening.

However, independent of the underlying marking strategy, we have a collection of cells marked for refinement or coarsening. In the case of pure h- or pure p-refinement, the error indicators provide sufficient refinement information. In the case of combined hp-refinement, however, we must decide *what* to refine and *how* to refine, namely to decide whether to apply h- or p-adaptivity.

Since the theoretical conditions for exponential convergence require a sufficient degree of local regularity [36], [37], we estimate the local smoothness on marked cells to decide h- over p-refinement and isolate non-smooth behavior. However, in contrast to existing works, we instead estimate the smoothness from the error in the field, which we extract from the DWR error estimation process; i.e., we leverage the field error between the two finite dimensional Galerkin approximate solutions (where one belongs to an enriched space) computed as part of evaluating the eigenvalue QoI error estimate in (12). While estimating directly from the solution provides effective refinement classification information, estimating the smoothness of the error strongly targets our principal objective: eliminating discretization error where the solution yields inadequate accuracy. Examining the smoothness of the error provides a more apt indicator for h-refinement as it marks where the error is due to the insufficient (local) smoothness. We adopt the approach demonstrated in [26] for estimating the decay of the Legendre expansion. The error field, keeping in mind the necessity of approximating the exact solution, is simply $(\mathbf{u}_{hp^+} - \mathbf{u}_{hp}) \in B_{hp^+}$ as $B_{hp} \subset B_{hp^+}$ (by construction). Hence, for each shape function $\hat{\boldsymbol{\varphi}}_j$ on every cell K, we have an associated error coefficient $e_{j,K}$. The Legendre coefficients of the w-component (e.g., the x- or y-components) of this local error field are then computed from

$$c_{\boldsymbol{\xi},K,w} = \sum_j \hat{L}_{i(\boldsymbol{\xi})j,w} e_{j,K} \tag{18}$$

$$\hat{L}_{i(\boldsymbol{\xi})j,w} = \left(\prod_{n \in \boldsymbol{\xi}} \frac{2n+1}{2} \right) \int_{\hat{K}} \hat{\varphi}_{j,w}(\hat{\mathbf{x}}) P_{\boldsymbol{\xi}}(\hat{\mathbf{x}}) J_K \, d\hat{\mathbf{x}}, \tag{19}$$

where $\hat{\varphi}_{j,w}$ indicates that the w-component of the vectorial shape function $\hat{\boldsymbol{\varphi}}_j$ is taken, J_K denotes the Jacobian determinant of the mapping between the reference cell and its image K, and the integrals in the transformation matrix $\hat{L}_{ij,w}$ are computed over the reference cell $\hat{K}$, where $P_{\boldsymbol{\xi}}$ denotes the tensor-product Legendre polynomial of the multi-index $\boldsymbol{\xi} \in \mathbb{N}_0^d$. The decay rate of each field component is estimated independently through linear regression of the logarithm of the coefficients, with the smallest predicted decay rate (which suggests lower regularity) propagated forward for refinement classification as we consider only isotropic refinements in this work. With support for anisotropic hp-refinements, the individual decay rates may be applied to instruct directional refinements instead. Of course, the expansion must be truncated to a finite number of terms. Hence, from [26], [38], we perform linear regression on the set of (modified) coefficients

$$C_{K,w} = \left\{ \log \left(\max_{\substack{\hat{\boldsymbol{\xi}} \\ \|\hat{\boldsymbol{\xi}}\|_1 = \|\boldsymbol{\xi}\|_1}} |c_{\boldsymbol{\xi},K,w}| \right) : \|\boldsymbol{\xi}\|_1 \leq p_K \right\}, \quad (20)$$

where p_K denotes the degree of the polynomial basis on cell K.

As in error estimation and marking cells for refinement or coarsening, each cell must be classified for h- or p-refinement. Analogously to the relative marking of cells, typical strategies employed rely on a relative threshold for determination, i.e., taking a threshold T such that

$$T(\kappa) = \kappa \eta_{max} + (1 - \kappa)\eta_{min}, \quad (21)$$

where $\kappa \in [0, 1]$ and η_{max} and η_{min} denote, respectively, the maximum and minimum decay rates. This form of the refinement classifier indicates a strong dependence on κ, with $\kappa = 0$ implying p-refinement only and $\kappa = 1$ implying h-refinement only, and therefore the need for a judicious choice. Typically, in the absence of prior information, $\kappa = 1/2$ is chosen; however, depending on the problem, we might expect additional value for p-refinement as opposed to h, and vice versa, motivating the need for an alternative classifier.

Instead, we take the approach as in [25], with a fixed threshold, such as $T = 1.0$. We find that when applying the Legendre smoothness indicator, $T = 1.0$ underestimates the smoothness, driving, therefore, less p-refinement than would be profitable. As a result, in the numerical results section, we take $T = 0.85$ as a more aggressive (in terms of p-refinement) yet still widely applicable tolerance. Naturally, a threshold too strongly weighted towards p-refinement or towards h-refinement will, in either case, inhibit the ability of the adaption algorithm to yield exponential convergence.

We summarize the adaptive error control procedure as follows:

1) For each cell, compute error contribution estimates and refinement indicators by means of (12) and (13)
2) Of the N total cells in the discretization, identify the m cells that should be refined, the l cells to coarsen, and the $N - m - l$ cells that are left unchanged
   a) Set m to be the minimizer of the objective function (16)
   b) With m now fixed, set l to be the minimizer of the objective function (17)
3) With the cells classified for refinement and coarsening, for each cell K, estimate the smoothness of the error field to determine whether the cell should be h- or p-refined/reduced
   a) On cell K, compute the difference $\mathbf{u}_{hp^+} - \mathbf{u}_{hp}$, associating the resulting error coefficients $e_{j,K}$ with each shape function $\hat{\boldsymbol{\varphi}}_j$ on cell K in the enriched finite element space
   b) Estimate the decay rate $C_{K,w}$ of the coefficients of the Legendre expansion using (20) for each component w of the error field (i.e., the vectorial directions)
      i) For isotropic refinements, take the only the minimum decay rate over the individual vectorial components of the error field
   c) If cell K is marked for refinement, then p-refine for a decay rate above some threshold T (e.g., $T = 1.0$ or $T = 0.85$); otherwise, h-refine
   d) If cell K is marked for coarsening, then coarsen in p for a decay rate below T; otherwise, coarsen in h

Note that for the actual execution of refinement or coarsening of the discretization, additional requirements that depend on the underlying hp-refinement implementation—such as maintenance of a 1-irregularity rule (i.e., only one hanging node per edge after an h-refinement)—require additional care, for example, as discussed in [39].

Finally, to analyze the effectiveness of proposed refinement, specifically for 2-D problems, we note that the relative error of the approximate eigenvalue is bounded by

$$Ce^{-b(\text{NDoFs})^{\kappa}}, \quad (22)$$

where NDoFs signifies the number of degrees of freedom, C, b, $\kappa > 0$ are constants independent of the NDoFs [17]. In 2-D, when the solution is smooth, $\kappa = 1/2$, otherwise $\kappa = 1/3$. A linear trend of the relative error (in log-scale) with respect to $(\text{NDoFs})^{\kappa}$ indicates exponential convergence, permitting a convenient method to visualize the performance of an adaptive strategy.

III. Numerical Results

We now apply the proposed adaptive mesh refinement procedure to a challenging model problem in the form of an L-shaped waveguide originally proposed by [40]. The implementation is based on the finite element library deal.II [10], [11], leveraging a continuous Galerkin approach with higher order Nédélec cells of the first kind [41] with support for non-uniform expansion orders and hanging-nodes (1-irregular) [9]. Visualization of the discretizations and the eigenfunctions was performed using VisIt [42].

From [40], [43] we have a collection of numerical reference eigenvalues to compare the accuracy and effectiveness of the proposed approach to adaptive hp-refinement in CEM.

In all examples, the starting geometric discretization is that of Fig. 1. The error in a given eigenvalue is computed from

This article has been accepted for publication in IEEE Transactions on Antennas and Propagation. This is the author's version which has not been fully edited and content may change prior to final publication. Citation information: DOI 10.1109/TAP.2022.3145473

(12), and the cells to refine and coarsen are chosen through successive minimization of the objective functions (16) and (17) under the assumption of the need to h-refine only. The marking strategy is then followed by recategorization of the refinement and coarsening to the isotropic h and p decisions according to the smoothness estimation outlined in Section II.

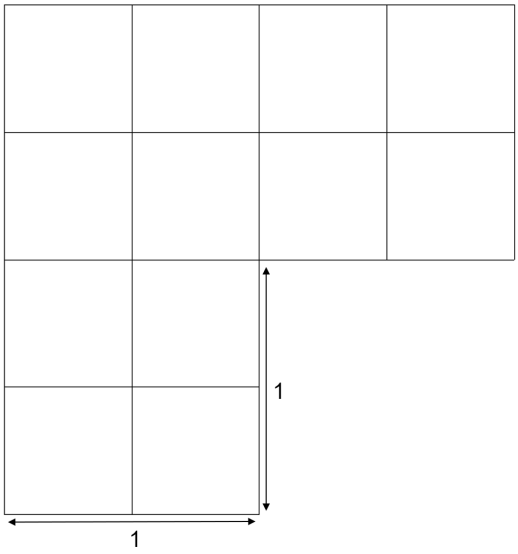

Fig. 1. The starting discretization for the L-shaped waveguide.

We focus our study on the smallest nine eigenvalues, the first five of which have been examined previously in [40], [43].

The first nine eigenpairs separate equally into three classes: those with strongly singular eigenfunctions, seen in Fig. 2; non-smooth eigenfunctions, seen in Fig. 3; and globally smooth eigenfunctions, seen in Fig. 4. The 1st, 6th, and 8th eigenpairs have highly singular eigenfunctions; the 2nd, 5th, and 9th eigenfunctions, while not unbounded, exhibit non-smooth behavior near the re-entrant corner of the domain; and the 3rd, 4th, and 7th eigenfunctions are globally smooth. Furthermore, note that in each case, the curl of the eigenfunction, which is purely in the axial direction, is non-zero. For the non-smooth and singular eigenfunctions, the curl is highly sensitive in a neighborhood about the re-entrant corner (i.e., small perturbations in position result in relatively large changes in the magnitude of the curl), though approximately zero at the re-entrant corner itself. The L-shaped waveguide, therefore, provides an excellent test case for the analysis of hp-refinement methods in CEM, providing a range of solution types to evaluate efficacy and efficiency.

For each class of eigenpair, we demonstrate the effectiveness of the proposed approach for hp-refinement. Based on the numerical experiments in [29], which indicated that accurate results typically require at least cubic or quartic polynomial bases, we initialize the primal discretization with uniformly cubic basis functions for the singular class and quartic for the non-smooth and smooth classes; however, the polynomial order may be reduced to unity through coarsening (i.e., the degree of coarsening in p is unrestricted), and the maximal

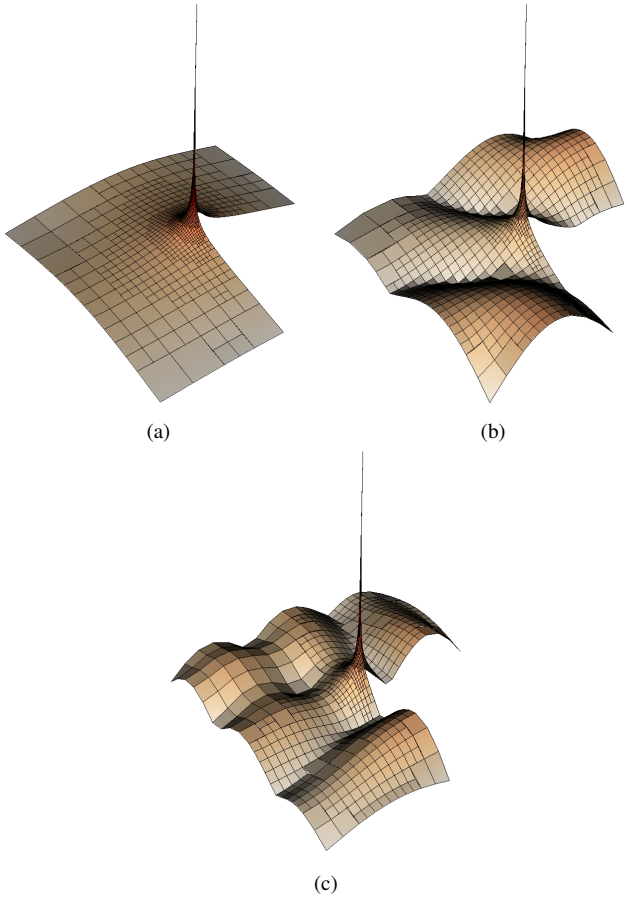

Fig. 2. Field magnitudes for the singular eigenfunctions. (a) The 1st eigenfunction. (b) The 6th eigenfunction. (c) The 8th eigenfunction.

expansion order for the primal discretization is limited to twelve. Note that initialization with linear basis functions is undesirable due to inadequate information for smoothness estimation [26]. For illustration of the advantage of estimation of the error smoothness over the solution smoothness, we include results from both strategies. We denote the error smoothness and the solution smoothness AMR strategies by E-AMR and S-AMR, respectively. The values of the eigenvalues include the correction term provided by the DWR and the increased cost (in terms of the number of degrees of freedom) to compute this estimate.

Starting with the singular class of eigenfunctions, the field magnitude is characterized by a singularity at the re-entrant corner and, depending on the mode, variation elsewhere in the domain. While the neighborhood around the re-entrant corner significantly influences the accuracy of the eigenvalues, it is not solely responsible; this presents tremendous challenge in highly accurate computations, and, in particular, prevents standard error indication strategies (e.g., the gradient-jump methods) from attaining maximum accuracy as the adaptivity will over-emphasize the re-entrant corner (to the neglect of the remainder of the discretization).

Fig. 5 depicts the results of the E-AMR and S-AMR procedures applied to the eigenpairs with singular eigenfunctions. For the convergence of the 1st eigenvalue, the presented E-AMR scheme provides significant improvements in efficiency,

This article has been accepted for publication in IEEE Transactions on Antennas and Propagation. This is the author's version which has not been fully edited and content may change prior to final publication. Citation information: DOI 10.1109/TAP.2022.3145473

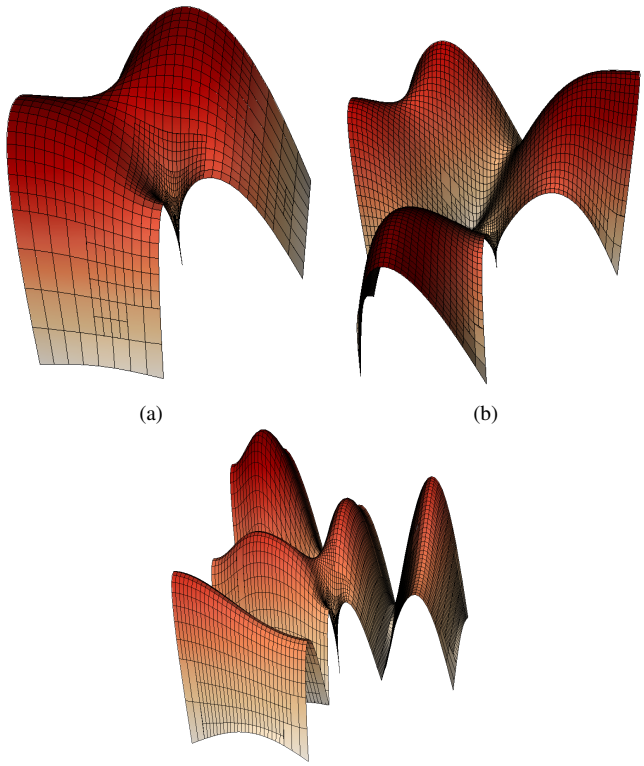

(a) (b) (c)

Fig. 3. Field magnitudes for the non-smooth eigenfunctions. (a) The 2nd eigenfunction. (b) The 5th eigenfunction. (c) The 9th eigenfunction.

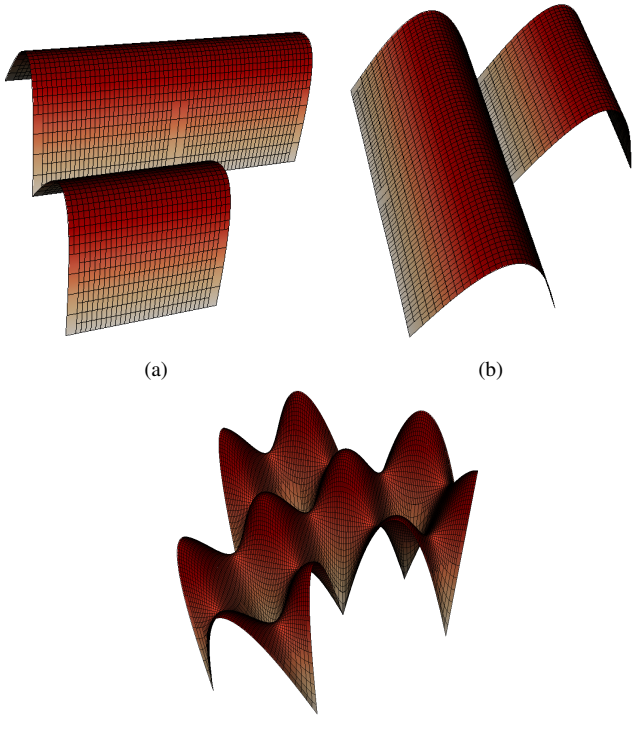

(a) (b) (c)

Fig. 4. Field magnitudes for the globally smooth eigenfunctions. (a) The 3rd eigenfunction. (b) The 4th eigenfunction. (c) The 7th eigenfunction.

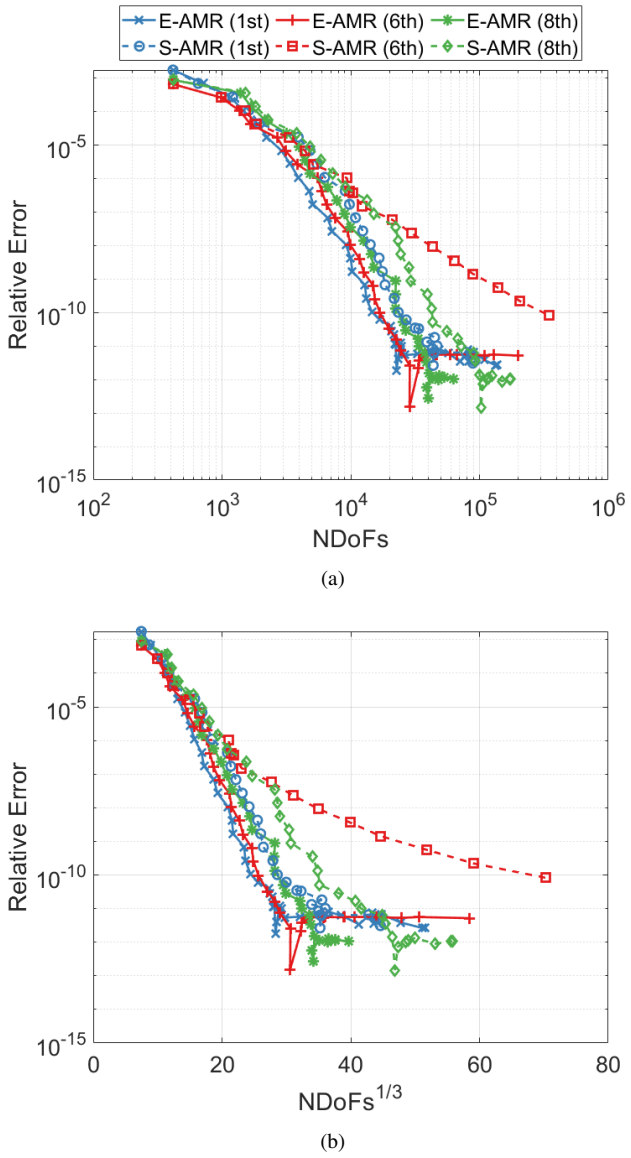

(a) (b)

Fig. 5. Convergence of the eigenvalues of the singular eigenfunctions with respect to the number of degrees of freedom. (a) Double logarithmic representation. (b) log-cube-root representation.

providing a 10 to 100 times improvement in the accuracy for the same number of DoFs compared to S-AMR. With the horizontal axis in Fig. 5(b) scaled with respect to $(\text{NDoFs})^{1/3}$, we see that E-AMR and S-AMR yield exponential convergence. Both approaches match the accuracy (12 digits) of the most accurate benchmark available [43], which required 59459 degrees of freedom. The E-AMR approach, however, required only 20364 DoFs to attain the same accuracy.

Moving on to the 6th eigenpair, we again see in Fig. 5 the advantage of the E-AMR approach. As no previous benchmark exists for this eigenpair, the reference value is taken from the invariant digits of the refinement process. With E-AMR, the convergence of the eigenvalue is nearly identical to the 1st eigenvalue, even with the increased fluctuation throughout the domain. S-AMR, however, is severely limited by estimating the smoothness from the solution, achieving only algebraic

This article has been accepted for publication in IEEE Transactions on Antennas and Propagation. This is the author's version which has not been fully edited and content may change prior to final publication. Citation information: DOI 10.1109/TAP.2022.3145473

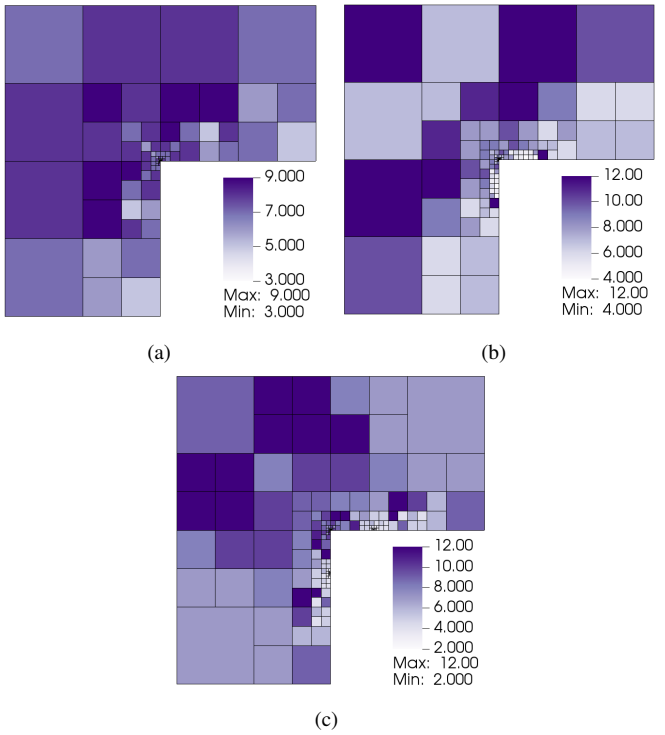

Fig. 6. The first converged discretizations for the singular eigenpairs. (a) The 1st eigenpair. (b) The 6th eigenpair. (c) The 8th eigenpair.

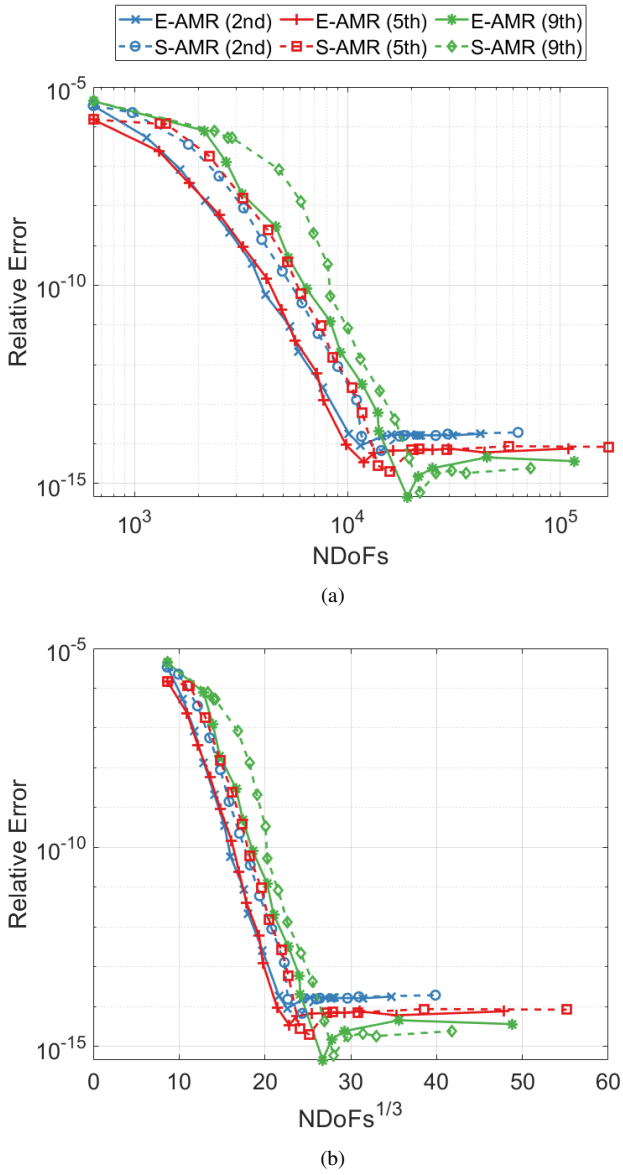

Fig. 7. Convergence of the eigenvalues of the non-smooth eigenfunctions with respect to the number of degrees of freedom. (a) Double logarithmic representation. (b) log-cube-root representation.

convergence with respect to the number of degrees of freedom for this eigenvalue, as seen in Fig. 5(b). Fully leveraging the information provided by the DWR process, as in the E-AMR strategy, produces exponential convergence without difficulty. Moreover, estimating the smoothness from the error, rather than the solution as is typical, produces discretizations several orders of magnitude more efficient. The E-AMR strategy reaches 12 digits of accuracy for this eigenvalue.

The 8th eigenpair produces similar results as to the 1st eigenpair; however, as the eigenpair itself is much more demanding in terms of computational resources, 38966 DoFs are required for 12 digits of precision using the proposed E-AMR strategy, whereas S-AMR requires nearly three times as many degrees of freedom for the same accuracy at 105840 DoFs. Furthermore, while E-AMR yields consistent exponential convergence, S-AMR performs inconsistently.

The first converged discretizations produced by E-AMR for the eigenvalues belonging to the singular class are shown in Fig. 6. For the 1st eigenvalue, shown in Fig. 6(a), the minimum and maximum expansion orders attained were three and nine, respectively. For the 6th eigenvalue, shown in Fig. 6(b), the minimum and maximum expansion orders were four and twelve, while the minimum and maximum for the 8th eigenpair, from Fig. 6(c), was two and twelve. All three problems resulted in a significant increase in cell density in the neighborhood of the singularity and large expansion orders where the eigenfunctions vary smoothly.

Repeating the same process but for the class of non-smooth eigenfunctions, we see similar performance. In each case the reference value for computing the relative error is taken from the invariant digits of the refinement process. As seen in Fig. 7, the E-AMR procedure achieves exponential convergence for each of the eigenvalues. S-AMR, while also yielding exponential convergence (apart from the early iterations for the 9th eigenvalue), is once again 10 to 100 times less efficient than the proposed E-AMR approach. Each approach, however, can provide 14 digits of accuracy. When examining the convergence of the 9th eigenvalue with S-AMR, estimating the smoothness of the solution results in substantially more h-refinement than necessary, reducing the efficiency in comparison to E-AMR.

Illustrated in Fig. 8, the first converged discretizations convey the increased rate of p-refinement possible for the non-smooth eigenfunctions in comparison to the singular eigenfunctions. The discretizations, however, still exhibit increased cell density at the re-entrant corner, given the sharp field behavior as seen in Fig. 3. The 9th eigenvalue requires a high

This article has been accepted for publication in IEEE Transactions on Antennas and Propagation. This is the author's version which has not been fully edited and content may change prior to final publication. Citation information: DOI 10.1109/TAP.2022.3145473

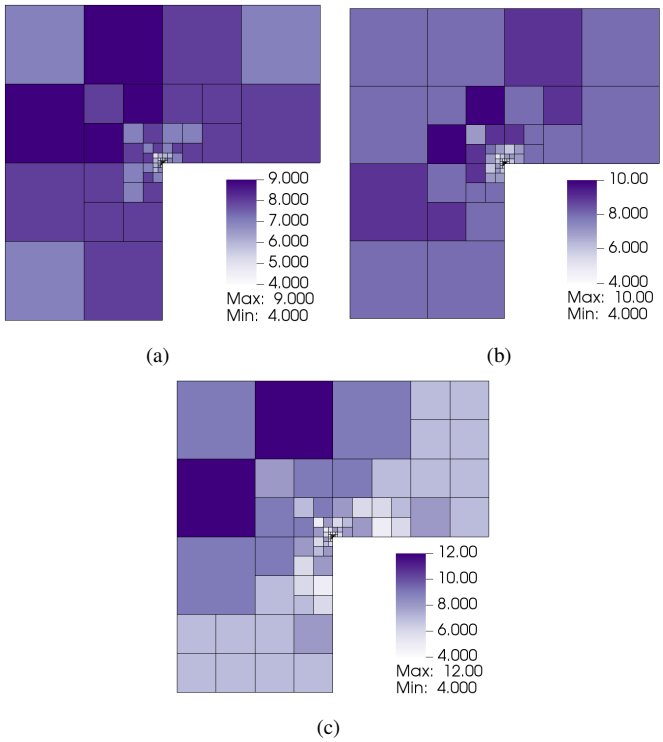

Fig. 8. The first converged discretizations for the non-smooth eigenpairs. (a) The 2nd eigenpair. (b) The 5th eigenpair. (c) The 9th eigenpair.

level of refinement globally, while the 2nd and 5th eigenvalues converge much earlier in terms of the number of degrees of freedom.

Finally, in the case of the three globally smooth eigenpairs, the eigenvalues converge to multiples of π^2. The 3rd and 4th eigenpairs, as identified by [40], share an eigenvalue of π^2 and the proposed E-AMR procedure indicates that the 7th eigenpair has an eigenvalue of $2\pi^2$.

Unsurprisingly, given the simplicity of the eigenfunctions depicted in Fig. 4(a)-(b), the E-AMR and S-AMR approaches perform identically for the 3rd and 4th eigenpairs, as depicted in Fig. 9, since both successfully detect the global smoothness and only p-refine each iteration. Note that for this case, the horizontal axis in Fig.9(b) is scaled with $\text{NDoFs}^{1/2}$ as the solutions are globally smooth and therefore $\kappa = 1/2$ in (22).

In contrast, the 7th eigenpair, which, like the 3rd and 4th eigenpairs, has a globally smooth eigenfunction, causes difficulty for the S-AMR strategy due to the rapid variations present in the mode, as shown in Fig. 4(c). E-AMR, on the other hand, once again drives only p-refinements each iteration for this eigenpair.

While the E-AMR yields exponential convergence and, most importantly, only conducts p-refinement (the ideal choice for the problem), estimating the smoothness from the solution as in S-AMR results in ineffectual h-refinements and fewer p-refinements in the early iterations, limiting the performance.

As the discretizations produced by E-AMR only require global p-refinement of the starting discretization (Fig. 1) at each iteration, and no h-refinements are performed to attain maximal accuracy, an illustration is omitted for the smooth eigenfunction class. For each of the three eigenpairs in this

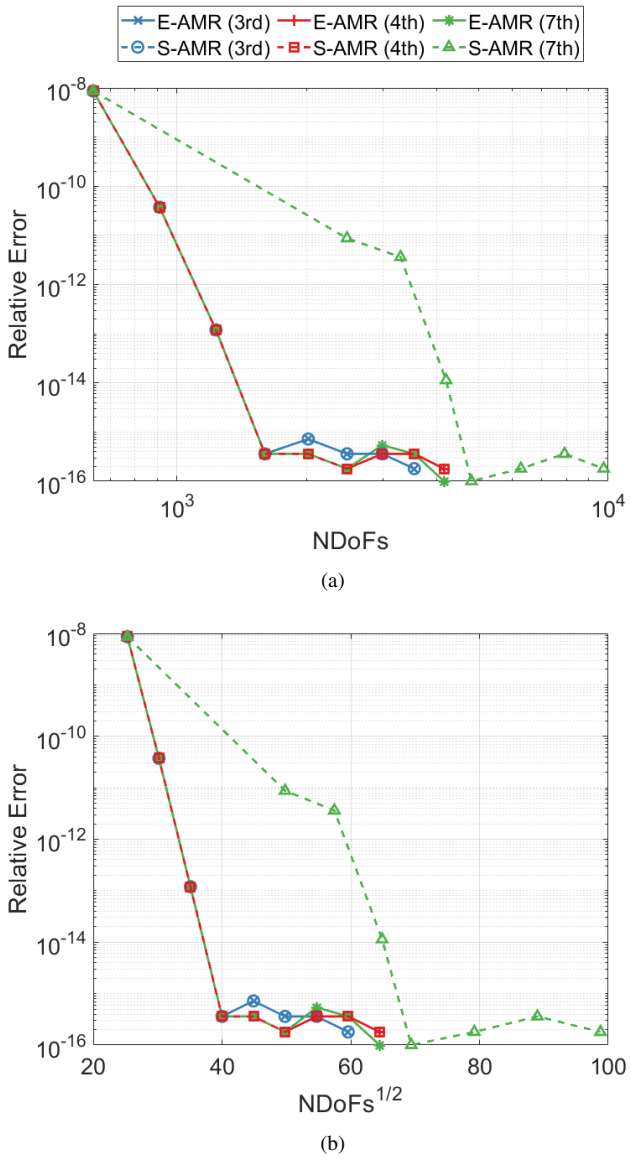

Fig. 9. Convergence of the eigenvalues of the smooth eigenfunctions with respect to the number of degrees of freedom. (a) Double logarithmic representation. (b) log-square-root representation.

class, convergence within machine precision for the eigenvalue computed using E-AMR to the reference value occurs for a uniform expansion order of $p = 7$ throughout the discretization.

Overall, the proposed adaption mechanism facilitates rapid convergence of the eigenvalue QoIs. By estimating the smoothness of the error, as in the E-AMR approach, exponential convergence was achieved across all examples tested. S-AMR, on the other hand, by estimating the smoothness of the solution, yielded acceptable, though less efficient, results for lower-order modes and demonstrated inconsistencies for the higher-order modes. As the field error is available from the computation of the DWR, E-AMR provides a significant enhancement of discretization quality without incurring substantial additional computational expenses in the refinement process.

Finally, in Table I we summarize the computed eigenvalues to expand upon existing benchmarks. The benchmark values were extracted from the E-AMR refinement process and each eigenvalue has an estimate of the number of accurate digits (i.e., the digits which are invariant under further refinements), as well as the previous best accuracy from available benchmarks (if applicable).

TABLE I
BENCHMARK EIGENVALUES COMPUTED WITH E-AMR.

Eigenvalue	Digits	Previous Digits [43]
1.47562182397	12	12
3.5340313667880	14	12
π^2	-	-
π^2	-	-
11.389479397947	14	12
12.5723873200	12	N/A
$2\pi^2$	-	N/A
21.4247335393	12	N/A
23.344371957137	14	N/A

IV. CONCLUSION

We have demonstrated the capability to adaptively refine from coarse initial discretizations to highly accurate eigenvalue computations through a combination of goal-orientated error estimation, intelligent refinement selection, and smoothness indication of the error, rather than the solution itself.

We applied the proposed approach to the first nine eigenpairs of a challenging waveguide model, including three singular, three non-smooth, and three smooth eigenfunctions. The E-AMR procedure achieved exponential convergence with respect to the number of degrees of freedom, permitting rapid refinement even for eigenpairs with singular eigenfunctions. In contrast, estimation of the smoothness of the solution in the S-AMR approach resulted in a large reduction in efficiency across all examples. Moreover, while achieving exponential convergence for lower-order modes, for the higher-order modes, S-AMR overestimated the need for h-refinement, resulting in reduced convergence rates.

In addition to confirming and improving the results of previous numerical benchmarks, we expanded the current set of benchmarks with higher-order modes for more challenging test cases. Furthermore, the extensions to higher-order modes illustrate the importance of including rapid (yet smooth) variation in the testing and design of hp-refinement algorithms.

Future works will study alternative approaches to the hp-decision to reduce sensitivity to the choice of the smoothness tolerance and, most importantly, to facilitate efficient applications with arbitrarily shaped cells.

ACKNOWLEDGMENT

The authors would like to thank Prof. Wolfgang Bangerth for helpful suggestions and valuable discussions.

REFERENCES

[1] W. Bangerth and R. Rannacher, *Adaptive Finite Element Methods for Differential Equations*. Birkhauser Basel, 2003.

[2] D. Estep, M. Holst, and D. Mikulencak, "Accounting for stability: a posteriori error estimates based on residuals and variational analysis," *Communications in Numerical Methods in Engineering*, vol. 18, no. 7, pp. 15–30, July 2002.

[3] K. Eriksson, D. Estep, P. Hansbo, and C. Johnson, "Introduction to adaptive methods for differential equations," *Acta Numerica*, vol. 4, p. 105–158, 1995.

[4] I. Babuška and M. R. Dorr, "Error estimates for the combined h and p versions of the finite element method," *Numerische Mathematik*, vol. 37, pp. 257–277, 06 1981.

[5] W. Gui and I. Babuška, "The h, p and h-p versions of the finite element method in 1 dimension, Part I." *Numerische Mathematik*, vol. 49, no. 6, pp. 577–612, Nov 1986.

[6] W. Gui and I. Babuška, "Theh, p and h-p versions of the finite element method in 1 dimension, Part II." *Numerische Mathematik*, vol. 49, no. 6, pp. 613–657, Nov 1986.

[7] W. Gui and I. Babuška, "The h, p and h-p versions of the finite element method in 1 dimension, Part III." *Numerische Mathematik*, vol. 49, no. 6, pp. 659–683, Nov 1986.

[8] I. Babuška and E. Rank, "An expert-system-like feedback approach in the hp-version of the finite element method," *Finite Elements in Analysis and Design*, vol. 3, no. 2, pp. 127–147, 1987.

[9] W. Bangerth and O. Kayser-Herold, "Data structures and requirements for hp finite element software," *ACM Trans. Math. Softw.*, vol. 36, no. 1, Mar. 2009.

[10] D. Arndt, W. Bangerth, B. Blais, T. C. Clevenger, M. Fehling, A. V. Grayver, T. Heister, L. Heltai, M. Kronbichler, M. Maier, P. Munch, J.-P. Pelteret, R. Rastak, I. Thomas, B. Turcksin, Z. Wang, and D. Wells, "The `deal.II` library, version 9.2," *Journal of Numerical Mathematics*, vol. 28, no. 3, pp. 131–146, 2020. [Online]. Available: https://dealii.org/deal92-preprint.pdf

[11] D. Arndt, W. Bangerth, D. Davydov, T. Heister, L. Heltai, M. Kronbichler, M. Maier, J.-P. Pelteret, B. Turcksin, and D. Wells, "The deal.II finite element library: Design, features, and insights," *Computers & Mathematics with Applications*, vol. 81, pp. 407–422, 2021. [Online]. Available: https://arxiv.org/abs/1910.13247

[12] F. Kikuchi, "On a discrete compactness property for the Nedelec finite elements," *J. Fac. Sci. Univ. Tokyo, Sect. IA. Math.*, vol. 36, pp. 479–490, 1989.

[13] D. Boffi, M. Costabel, M. Dauge, L. F. Demkowicz, and R. Hiptmair, "Discrete compactness for the p-version of discrete differential forms," *SIAM Journal on Numerical Analysis*, vol. 49, no. 1, pp. 135–158, 2011.

[14] D. Boffi, M. Costabel, M. Dauge, and L. F. Demkowicz, "Discrete compactness for the hp version of rectangular edge finite elements," *SIAM Journal on Numerical Analysis*, vol. 44, no. 3, pp. 979–1004, 2006.

[15] M. M. Ilic, A. Z. Ilic, and B. M. Notaroš, "Efficient large-domain 2-D FEM solution of arbitrary waveguides using p-refinement on generalized quadrilaterals," *IEEE Transactions on Microwave Theory and Techniques*, vol. 53, no. 4, pp. 1377–1383, 2005.

[16] D. Boffi and L. Gastaldi, "Adaptive finite element method for the Maxwell eigenvalue problem," *SIAM Journal on Numerical Analysis*, vol. 57, 04 2018.

[17] J. Coyle and P. D. Ledger, "Evidence of exponential convergence in the computation of Maxwell eigenvalues," *Computer Methods in Applied Mechanics and Engineering*, vol. 194, pp. 587–604, 02 2005.

[18] M. Ainsworth, J. Coyle, P. D. Ledger, and K. Morgan, "Computing Maxwell eigenvalues by using higher order edge elements in three dimensions," *IEEE Transactions on Magnetics*, vol. 39, no. 5, pp. 2149–2153, 2003.

[19] L. F. Demkowicz, "Fully automatic hp-adaptivity for Maxwell's equations," *Computer Methods in Applied Mechanics and Engineering*, vol. 194, no. 2, pp. 605 – 624, 2005.

[20] D. Pardo and L. F. Demkowicz, "Integration of hp-adaptivity and a two-grid solver for elliptic problems," *Computer Methods in Applied Mechanics and Engineering*, vol. 195, no. 7, pp. 674–710, 2006.

[21] L. E. G. Castillo, D. Pardo, and L. F. Demkowicz, "Fully automatic hp adaptivity for electromagnetics, application to the analysis of H-plane and E-plane rectangular waveguide discontinuities," in *2007 IEEE/MTT-S International Microwave Symposium*, 2007, pp. 285–288.

[22] L. E. Garcia-Castillo, D. Pardo, and L. F. Demkowicz, "Energy-norm-based and goal-oriented automatic hp adaptivity for electromagnetics:

Application to waveguide discontinuities," *IEEE Transactions on Microwave Theory and Techniques*, vol. 56, no. 12, pp. 3039–3049, 2008.
[23] D. Pardo, L. E. García-Castillo, L. F. Demkowicz, and C. Torres-Verdín, "A two-dimensional self-adaptive hp finite element method for the characterization of waveguide discontinuities. Part II: Goal-oriented hp-adaptivity," *Computer Methods in Applied Mechanics and Engineering*, vol. 196, no. 49, pp. 4811–4822, 2007.
[24] M. Bürg, "Convergence of an automatic hp-adaptive finite element strategy for Maxwell's equations," *Applied Numerical Mathematics*, vol. 72, pp. 188–204, 10 2013.
[25] C. Mavriplis, "Adaptive mesh strategies for the spectral element method," *Computer Methods in Applied Mechanics and Engineering*, vol. 116, no. 1, pp. 77–86, 1994.
[26] M. Fehling, "Algorithms for massively parallel generic hp-adaptive finite element methods," Ph.D. dissertation, Univ. Wuppertal, 2020.
[27] P. Houston, B. Senior, and E. Süli, "Sobolev regularity estimation for hp-adaptive finite element methods," *Numerical Mathematics and Advanced Applications*, pp. 619–644, 2003.
[28] C. Key, A. Smull, D. Estep, T. Butler, and B. M. Notaroš, "A posteriori error estimation and adaptive discretization refinement using adjoint methods in CEM: A study with a one-dimensional higher-order fem scattering example," *IEEE Transactions on Antennas and Propagation*, vol. 68, no. 5, pp. 3791–3806, 2020.
[29] J. J. Harmon, C. Key, D. Estep, T. Butler, and B. M. Notaroš, "Adjoint-based accelerated adaptive refinement in frequency domain 3-D finite element method scattering problems," *IEEE Transactions on Antennas and Propagation*, vol. 69, no. 2, pp. 940–949, 2021.
[30] P. Arbenz, R. Geus, and S. Adam, "Solving Maxwell eigenvalue problems for accelerating cavities," *Phys. Rev. ST Accel. Beams*, pp. 1–10, 2001.
[31] L. Vardapetyan, L. F. Demkowicz, and D. P. Neikirk, "hp-vector finite element method for eigenmode analysis of waveguides," *Computer Methods in Applied Mechanics and Engineering*, vol. 192, pp. 185–201, 01 2003.
[32] V. Heuveline and R. Rannacher, "A posteriori error control for finite element approximations of elliptic eigenvalue problems," *J. Adv. Comp. Math*, vol. 15, pp. 107–138, 2001.
[33] L. E. García-Castillo, D. Pardo, I. Gómez-Revuelto, and L. F. Demkowicz, "A two-dimensional self-adaptive hp finite element method for the characterization of waveguide discontinuities. Part I: Energy-norm based automatic hp-adaptivity," *Computer Methods in Applied Mechanics and Engineering*, vol. 196, no. 49, pp. 4823–4852, 2007.
[34] T. Richter, "Parallel multigrid method for adaptive finite elements with application to 3D flow problems," Ph.D. dissertation, University of Heidelbergl, 2005.
[35] W. Rachowicz, "An anisotropic h-type mesh-refinement strategy," *Computer Methods in Applied Mechanics and Engineering*, vol. 109, no. 1, pp. 169–181, 1993.
[36] I. Babuška and M. Suri, "The p and h-p versions of the finite element method, basic principles and properties," *SIAM Review*, vol. 36, no. 4, pp. 578–632, 1994.
[37] B. Guo and I. Babuška, "The h-p version of the finite element method," *Computational Mechanics*, vol. 1, no. 1, pp. 21–41, 1986.
[38] T. Eibner and J. M. Melenk, "An adaptive strategy for hp-FEM based on testing for analyticity," *Comput Mesh*, vol. 39, no. 39, pp. 575–595, 2007.
[39] W. Bangerth, C. Burstedde, T. Heister, and M. Kronbichler, "Algorithms and data structures for massively parallel generic adaptive finite element codes," *ACM Trans. Math. Softw.*, vol. 38, no. 2, pp. 1–28, 2012.
[40] M. Dauge, "Benchmark computations for Maxwell equations for the approximation of highly singular solutions," https://perso.univ-rennes1.fr/monique.dauge/benchmax.html, 2004.
[41] J. C. Nédélec, "Mixed finite elements in $\mathbb{R}^3$," *Numerische Mathematik*, vol. 35, pp. 315–341, 1980.
[42] H. Childs, E. Brugger, B. Whitlock, J. Meredith, S. Ahern, D. Pugmire, K. Biagas, M. Miller, C. Harrison, G. H. Weber, H. Krishnan, T. Fogal, A. Sanderson, C. Garth, E. W. Bethel, D. Camp, O. Rübel, M. Durant, J. M. Favre, and P. Navrátil, "VisIt: An End-User Tool For Visualizing and Analyzing Very Large Data," in *High Performance Visualization–Enabling Extreme-Scale Scientific Insight*, Oct 2012, pp. 357–372.
[43] M. Duruflé, "Benchmark computations for Maxwell equations for the approximation of highly singular solutions," https://www.math.u-bordeaux.fr/~durufle/eigenvalue.php, 2006.

Jake J. Harmon (S'19) was born in Fort Collins, CO in 1996. He received the B.S. degree (*summa cum laude*) in Electrical Engineering from Colorado State University, Fort Collins, CO, USA, in 2019, where he is currently pursuing the Ph.D. degree in Electrical Engineering.

His current research interests include adaptive numerical methods, uncertainty quantification, computational geometry, and higher order modeling in the finite element method and surface integral equation method of moments.

Branislav M. Notaroš (M'00–SM'03–F'16) received the Dipl.Ing. (B.S.), M.S., and Ph.D. degrees in electrical engineering from the University of Belgrade, Belgrade, Yugoslavia, in 1988, 1992, and 1995, respectively.

From 1996 to 1999, he was Assistant Professor in the School of Electrical Engineering at the University of Belgrade. He was Assistant and Associate Professor from 1999 to 2006 in the Department of Electrical and Computer Engineering at the University of Massachusetts Dartmouth. He is currently Professor of Electrical and Computer Engineering, University Distinguished Teaching Scholar, and Director of Electromagnetics Laboratory at Colorado State University.

Dr. Notaroš serves as General Chair of the 2022 IEEE International Symposium on Antennas and Propagation and USNC-URSI Radio Science Meeting and is Track Editor for the IEEE Transactions on Antennas and Propagation. He serves as President of Applied Computational Electromagnetics Society (ACES), as Chair of USNC-URSI Commission B, and as Meetings Committee Chair for the IEEE Antennas and Propagation Society. He was the recipient of the 2005 IEEE MTT-S Microwave Prize, 1999 IEE Marconi Premium, 2019 ACES Technical Achievement Award, 2015 ASEE ECE Distinguished Educator Award, 2015 IEEE Undergraduate Teaching Award, and many other research and teaching international and national awards.